machines

MDPI

Article

Robust Reduced-Order Active Disturbance Rejection Control Method: A Case Study on Speed Control of a One-Dimensional Gimbal

Fan Wang [1,2,3,†], Peng Liu [1,2,3,†], Meilin Xie [1,2,3], Feng Jing [1,2,3], Bo Liu [1,2,3], Yu Cao [1,2,3] and Caiwen Ma [1,2,3,*]

[1] Xi'an Institute of Optics and Precision Mechanics, Chinese Academy of Sciences, Xi'an 710119, China; wangfan@opt.ac.cn (F.W.); liupeng1@opt.ac.cn (P.L.); xiemeilin@opt.ac.cn (M.X.); jingfeng@opt.ac.cn (F.J.); liubo@opt.ac.cn (B.L.); caoyu@opt.ac.cn (Y.C.)
[2] School of Optoelectronics and Materials Science, University of Chinese Academy of Sciences, Beijing 100049, China
[3] Key Laboratory of Space Precision Measurement Technology, Chinese Academy of Sciences, Xi'an 710119, China
* Correspondence: cwma@opt.ac.cn; Tel.: +86-17392209365
† These authors contributed equally to this work.

Abstract: Usually, the order of active disturbance rejection control (ADRC) is equal to the relative order of the plant. To improve the control performance, a robust reduced-order method for ADRC is investigated in this paper. Firstly, frequency domain analysis shows that the lower-order extended state observer (ESO) has a smaller disturbance estimation error, so disturbance attenuation capability can be improved by reducing the order of ADRC. However, using only reduced-order ADRC will worsen the robustness of closed-loop systems. Therefore, a robust ADRC method based on a modified noise reduction disturbance observer (MNRDOB) is proposed. The main role of the MNRDOB is to improve the control performance of the closed-loop system by modifying the structure of the controlled object. In addition, the robust stability of the closed-loop control system based on the MNRDOB is discussed. Moreover, some simulations are used to demonstrate the robustness and noise suppression effects of the compound control method reduced-order ADRC with MNRDOB, and the parameter tuning method for the MNRDOB to improve the robustness of the system is given. Finally, some experiments on speed control of a one-dimensional gimbal are performed, and the results show that the proposed method is excellent in overshoot, tracking accuracy, and disturbance attenuation.

Keywords: reduced-order control; active disturbance rejection control (ADRC); disturbance observer (DOB); robust stability; one-dimensional gimbal

Citation: Wang, F.; Liu, P.; Xie, M.; Jing, F.; Liu, B.; Cao, Y.; Ma, C. Robust Reduced-Order Active Disturbance Rejection Control Method: A Case Study on Speed Control of a One-Dimensional Gimbal. *Machines* **2022**, *10*, 592. https://doi.org/10.3390/machines10070592

Academic Editors: Jan Gorecki, Mateusz Kukla and Maciej Berdychowski

Received: 25 June 2022
Accepted: 15 July 2022
Published: 20 July 2022

1. Introduction

Active disturbance rejection control (ADRC) as a robust control method can effectively overcome nonlinear dynamics, model uncertainty, and external disturbances [1,2]. ADRC control technology was first proposed by Prof. Han [3,4]. Its central idea is to use an extended state observer (ESO) to estimate the total disturbance including internal and external disturbances of the system, and then the estimation is used in feedback to compensate for disturbances. Gao proposed the linear ADRC for the purpose of simplifying parameter tuning and system performance analysis [5]. As a practical control solution, ADRC is applied to many engineering systems, such as motor drivers [6–8], underwater gliders [9,10], power systems [11], and the Piezoelectric Actuator System [12], etc.

The design process of the ADRC does not require detailed model information of the plant, except for the model order and control gain. Generally, the order of ADRC is required to be equal to the order of the plant to meet the need of disturbance estimation and

compensation. However, in some cases, the coefficients of the high-frequency components of the system are very small, and the plant model is usually simplified to a lower order to simplify controller design and performance analysis [13]. This simplification is very common in multi-closed-loop control systems in series, such as the three-loop servo control of the motor [14,15]. On the other hand, for some systems with complex dynamics, the real model order is difficult to obtain or may even be time-varying. In addition, a simplified model is also desirable for controller design and performance analysis. It is clear the ADRC designed by the simplified model is a reduced-order control scheme. However, there is no description of the advantages and disadvantages of this reduced-order control scheme in the existing literature. Three problems may limit the proposal of order-reduction schemes. One is that classical ADRC design methods usually show superior control performance. Secondly, the simplification of the controlled object model is very common in engineering applications, and this simplification is usually based on experience but very effective. Third, the reduced-order scheme will indeed reduce the robustness of the system. Although the reduced-order ESO has been widely studied [16,17], it is essentially a simplification based on the output differential of the system, and the order of ADRC composed of the reduced-order ESO remains unchanged. Although the reduced-order ESO has been widely studied, its essence is the simplification of ESO by means of a system output differential, and the order of the ADRC composed of the reduced-order ESO does not change. Therefore, the existing reduced-order ESO is irrelevant to the reduced-order ADRC scheme studied in this paper.

In this paper, the conditions of the reduced-order ADRC control scheme to stabilize the closed-loop system are clearly stated. In addition, the frequency domain analysis shows that the lower-order ESO has stronger disturbance estimation ability, which means that using a reduced-order ADRC can improve the anti-disturbance performance of the system. However, the reduced-order ADRC will reduce the system's robustness. It is also considered that sensor noise suppression is a constant subject for control systems. Therefore, a modified noise reduction disturbance observer (MNRDOB) is proposed to form the compound control strategy of reduced-order ADRC + MNRDOB. Note that the noise reduction disturbance observer (NRDOB) was first developed by [18]; however, two limitations lead to the fact that the NRDOB in [18] cannot be used to deal with defects in the reduced-order ADRC. On the one hand, the anti-disturbance capability of the NRDOB control system in [18] is determined only by the NRDOB and is independent of the nominal controller of the outer loop. Therefore, applying this NRDOB will offset the ADRC's advantage in disturbance rejection. On the other hand, the use of a reduced-order nominal model for NRDOB in [18] may destabilize the closed-loop system. In addition, [19] proposed a simplified NRDOB (SNRDOB), but the SNRDOB does not change the controlled object of the outer loop nominal controller in robust stability conditions, so it cannot improve the robustness of the reduced-order ADRC system. The MNRDOB proposed in this paper avoids these defects.

The objective of this paper is to clarify the significance and rationality of the reduced-order ADRC scheme that is common in engineering applications and to propose a robust control scheme to overcome the shortcomings of this reduced-order scheme. The simulations demonstrate the superiority of the proposed method in robustness and noise reduction. In addition, the proposed method is used for speed control of a one-dimensional gimbal to verify its effectiveness. The rest of the paper is arranged as follows. Section 2 introduces the ADRC algorithm and describes the conditions under which the reduced-order ADRC can stabilize the closed-loop system. In addition, the frequency domain analysis is utilized to show that the lower-order ESO has stronger perturbation estimation ability. In Section 3, an MNRDOB is proposed to improve system robustness and suppress sensor noise. The robust stability conditions of closed-loop systems are also discussed. In Section 4, the simulation analysis is carried out and the tuning method of MNRDOB parameters is given. Some experimental results are shown in Section 5. Section 6 concludes this paper.

2. ADRC Algorithm

2.1. Classical ADRC Algorithm

Consider the following single input single output linear system with disturbance

$$\begin{aligned} \dot{x}_1 &= x_2 \\ \dot{x}_2 &= x_3 \\ &\vdots \\ \dot{x}_n &= \alpha_1 x_1 + \alpha_2 x_2 + \cdots + \alpha_n x_n + b_n u_r + f_n \\ y &= x_1 \end{aligned} \tag{1}$$

where $x_i\,(i=1,2,\cdots,n)$ are the system states, $\alpha_i, i=1,2,...,n$ are constants, u_r is the control input, $f_n(t)$ is the total disturbance including unmodeled dynamics and external disturbance, $b_n > 0$ is the nominal control gain, and let $g_n(x)=\alpha_1 x_1 + \alpha_2 x_2 + \cdots + \alpha_n x_n$. By defining $x_{n+1} = f_n(t)$ as the total disturbance and letting $h_n(t) = \dot{f}_n(t)$, the dynamic system (1) can be rewritten as an extended model:

$$\begin{aligned} \dot{x}_1 &= x_2 \\ \dot{x}_2 &= x_3 \\ &\vdots \\ \dot{x}_n &= x_{n+1} + g_n(x) + b_n u_r \\ \dot{x}_{n+1} &= h_n \\ y &= x_1 \end{aligned} \tag{2}$$

The compact form of (2) can be described as

$$\begin{aligned} \dot{x}_e &= A_e x_e + B_e[g(x) + b_n u_r] + B_h h \\ y &= C_e x_e \end{aligned} \tag{3}$$

where $x_e = [x_1, x_2, \cdots, x_{n+1}]^T \in R^{n+1}$, $B_e = [0,0,\cdots,1,0]^T \in R^{n+1}$, and $B_h = [0,0,\cdots,1]^T \in R^{n+1}$, $C_e = [1,0,\cdots,0] \in R^{n+1}$.

According to (3) an n + 1st-order ESO is designed as

$$\dot{z}_e = A_e z_e + B_e b_n u_r + \beta e_1 \tag{4}$$

where $z_e = [z_1, z_2, \cdots, z_{n+1}]^T \in R^{n+1}$ is the output vector of ESO, $e_1 = x_1 - z_1$, and $\beta = [\beta_1, \beta_2, \cdots, \beta_{n+1}]^T \in R^{n+1}$ is observer gain vector and $\beta_i = \frac{(2+1)!}{i!(3-i+1)!}\omega_o^i, i=1,2,...,n$ as suggested by [5], $\omega_o > 0$ is the observer bandwidth to be designed. The corresponding n + 1st-order state error feedback (SEF) is

$$u_r = (K(v-z) - z_{n+1})/b_n \tag{5}$$

where $v = [v_1, v_2, \cdots, v_n]^T \in R^n$ is the output vector of the nth-order tracking differentiator (TD) [4], $z = [z_1, z_2, \cdots, z_n]^T \in R^n$, and $K = [k_1, k_2, \cdots, k_n] \in R^n$ is controller gain vector. The n + 1st-order ESO, the nth-order SEF, and the nth order TD constitute an nth-order ADRC. Subtract (4) from (3) and let $e = x_e - z_e$, and then the following error dynamics can be obtained.

$$\dot{e} = (A_e - \beta C_e)e + B_h h_n \tag{6}$$

Lemma 1. *For ω_o>0, the state e of (6) converges into a ball centered in the origin, if matrix $A_e - \beta C_e$ is Hurwitz and if there exists a constant L > 0 such that $|h_n| \le L$.*

The detailed proof process of Lemma 1 can be seen in [20], which will not be described in detail here.

Writing (1) as compact form

$$\dot{x} = Ax + Bu_r + B_f f_n \tag{7}$$

where $x = [x_1, x_2, \cdots, x_n]^T \in R^n$ is the state vector, $B = [0, 0, \cdots, b_n]^T \in R^n$, and $B_f = [0, 0, \cdots, 1]^T \in R^n$, it is easy to check that, for $|h_n| \le L$, if $A_e - \beta C$ and $A - BK/b$ are both stable, the closed loop system consisting of (5) and (7) is stable.

2.2. Reduced-Order ADRC Algorithm

It can be seen from the above derivation that, in the traditional design, the order of ADRC is equal to the order of the target plant. However, from Lemma 1, it is noted that the premise of the stability of the closed-loop system is $|h_n| \le L$ rather than directly related to the order. Therefore, as long as $|h_n| \le L$ is satisfied, it is feasible to design a low-order ADRC to control a high-order plant. The following assumptions are put forward.

Assumption 1. *The control input* u_r *and its derivative are bounded by*

$$|u_r| \le U < +\infty, \qquad |\dot{u}_r| \le \Delta U < +\infty \tag{8}$$

Assumption 2. *The total disturbance* $f_n(t)$ *is bounded by*

$$f_n(t) \le F < +\infty \tag{9}$$

Note that Assumption 2 may be somewhat conservative, because it may lead to non-convergence under state-dependent uncertainty shown in [21,22]. To overcome this conservatism, modeling and analysis of state-dependent uncertainty can be carried out by referring to the method in [21,22], which will not be described in detail here. In fact, one of the conditions established by ordinary ADRC is that the first derivative of the total perturbation is bounded, which is also conservative for state-dependent model uncertainties. Therefore, the analysis method on the uncertainty of the state-dependent model in [21,22] is of great significance to study the stability of ADRC.

The reduced-order model of the nth-order system (1) is as follows:

$$\begin{aligned} \dot{x}_1 &= x_2 \\ \dot{x}_2 &= x_3 \\ &\vdots \\ \dot{x}_{n-1} &= -\frac{1}{\alpha_n}\left(\alpha_1 x_1 + \alpha_2 x_2 + \cdots + \alpha_{n-1} x_{n-1} + f_n - \dot{x}_n\right) + b_{n-1} u_r \\ y &= x_1 \end{aligned} \tag{10}$$

where $b_{n-1} = -\frac{b_n}{\alpha_n}$. Equation (10) can be simplified as

$$\begin{aligned} \dot{x}_1 &= x_2 \\ \dot{x}_2 &= x_3 \\ &\vdots \\ \dot{x}_{n-1} &= \left[x_n - \Gamma(x) - b_{n-1} u_r\right] + \Gamma(x) + b_{n-1} u_r \\ y &= x_1 \end{aligned} \tag{11}$$

where

$$\dot{\Gamma}(x)=\frac{d\Gamma(x)}{dt}=\begin{cases} gx & , \ if \ \ Assumption 1 \ holds \\ gx+b_n u_r - b_{n-1}\dot{u}_r & , \ else \end{cases}$$

By defining $X_n = f_{n-1} = x_n - \Gamma(x) - b_{n-1}u_r$ as total disturbance of the reduced-order system and when Assumption 1 holds $h_{n-1}(t)=\dot{f}_{n-1}(t) = f_n - b_{n-1}\dot{u}_r + b_n u_r$ (when Assumption 1 does not hold $h_{n-1}(t)=\dot{f}_{n-1}(t) = f_n$), the extended model (nth-order model) of (11) is

$$\begin{aligned} \dot{x}_1 &= x_2 \\ \dot{x}_2 &= x_3 \\ &\vdots \\ \dot{x}_{n-1} &= \Gamma(x) + b_{n-1}u_r \\ \dot{X}_n &= h_{n-1} \\ y &= x_1 \end{aligned} \tag{12}$$

Proposition 1. *Based Assumption 2, according to the extended model (12) of the reduced-order model (10), an observer such as (4) can be designed for system (1), and for* $\omega_o > 0$*, the observation error converges in the ball centered at the origin.*

Proof of Proposition 1. *From Assumption 1 and Assumption 2, one has*

$$|h_{n-1}(t)| = \begin{cases} |f_n - b_{n-1}\dot{u}_r + b_n u_r| \le F + b_{n-1}\Delta U + b_n U, \ if \ \ Assumption 1 \ holds \\ |f_n| \le F \qquad\qquad\qquad\qquad\qquad\qquad , \ else \end{cases} \quad \square \tag{13}$$

Equation (13) means that the derivative of the total disturbance f_{n-1} is bounded. Then, Proposition 1 is easily proved by Lemma 1.

Remark 1. *It should be noted that it is necessary for* $b_{n-1} > 0$*, which means that* α_n *is a negative constant. It is worth emphasizing that the ESO designed according to the reduced-order model (10) and the extended model (12) is nth order, while the ESO designed by the classical method is n + 1st order. Therefore, the ESO designed according to Proposition 1 is of order reduced.*

Remark 2. *Proposition 1 implies that the condition of bounded estimation error of reduced-order ESO is different from that of classical ESO. The reduced-order ESO requires Assumption 2 to hold, while classical ESO requires bounded perturbation differentiation.*

Remark 3. *It is easy to check on the premise of satisfying Assumptions 1 and 2; the order of system (10) can be further reduced in the way of (10)-(12) to obtain the n-ith-order (i ≥ 1) model. According to Proposition 1, n-i + 1st-order ESO can be designed. This result explains why the ADRC system is still stable when a low-pass filter is connected in series.*

As the core of ADRC, ESO directly determines the control performance of ADRC. The lower-order ESO means smaller phase delay and more accurate disturbance estimation performance. Let us take the second-order ESO and third-order ESO as examples. Defining $\hat{f}$ as the estimate of f by ESO and letting $\tilde{f} = f - \hat{f}$, the transfer functions from f to $\tilde{f}$ for second- and third-order ESO, respectively, are obtained by the same method given in [23,24].

$$\frac{\tilde{f}}{f} = \frac{s^2 + \beta_1 s}{s^2 + \beta_1 s + \beta_2} = \frac{s^2 + 2\omega_o s}{(s+\omega_o)^2} \tag{14}$$

$$\frac{\tilde{f}}{f} = \frac{s^3 + \beta_1 s^2 + \beta_2 s}{s^3 + \beta_1 s^2 + \beta_2 s + \beta_3} = \frac{s^3 + 3\omega_o s^2 + 3\omega_o{}^2 s}{(s+\omega_o)^3} \tag{15}$$

According to the tuning method in [5], the bandwidth of the detector is set to ω_o=300*rad/s* . The amplitude-frequency characteristic plots of (9) and (10) are shown in Figure 1. We can see that in the low-frequency range, the amplitude attenuation ability of the second-order ESO is stronger than the third-order one, resulting in a smaller estimation error.

Remark 4. *The lower-order ESO has stronger disturbance estimation capability, which means the reduced-order ADRC has stronger disturbance attenuation capability. However, a reduced-order ADRC leads to a greater model error, i.e., a larger total disturbance. The larger the model error, the larger the observer bandwidth required. However, the excessive observer bandwidth will amplify the noise and cause the system performance to deteriorate. Thus, using reduced-order ADRC may cause less robustness. Therefore, ensuring system robustness is the prerequisite for using reduced-order ADRC.*

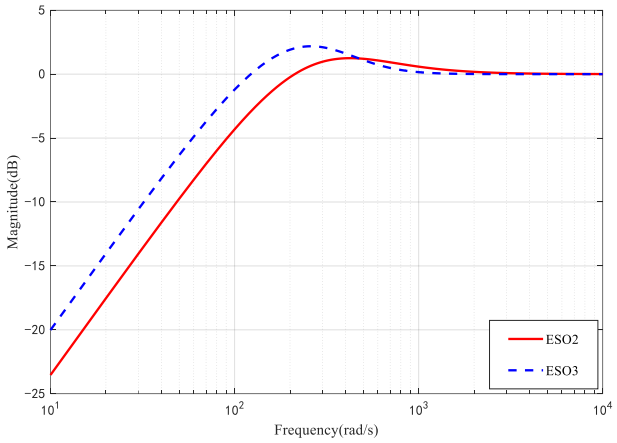

Figure 1. The amplitude-frequency characteristic plots for $\tilde{f}/f$ transfer functions.

3. MNRDOB-Based ADRC

3.1. Modified Noise Reduction Disturbance Observer

As described in Remark 4, the reduced-order ADRC may deteriorate the system robustness, so an additional algorithm is needed to overcome this problem. On the other hand, sensor noise in many control systems cannot be avoided, so it is an urgent problem to filter sensor noise in ADRC systems. In this section, a modified noise reduction disturbance observer (MNRDOB) is developed from [18] to suppress sensor noise and compensate for modeling errors and external disturbances.

To reduce noise in high-precision control, the noise reduction disturbance observer (NRDOB) was developed from the framework of the disturbance observer (DOB) [25], which clearly solves the attenuation of sensor noise at high frequency. NRDOB has been applied in series elastic actuator control, which significantly improves system stiffness [26]. The noise reduction of the NRDOB is achieved by transforming the actual system output into a dynamic model by using a nominal model. The NRDOB closed-loop system is shown in Figure 2.

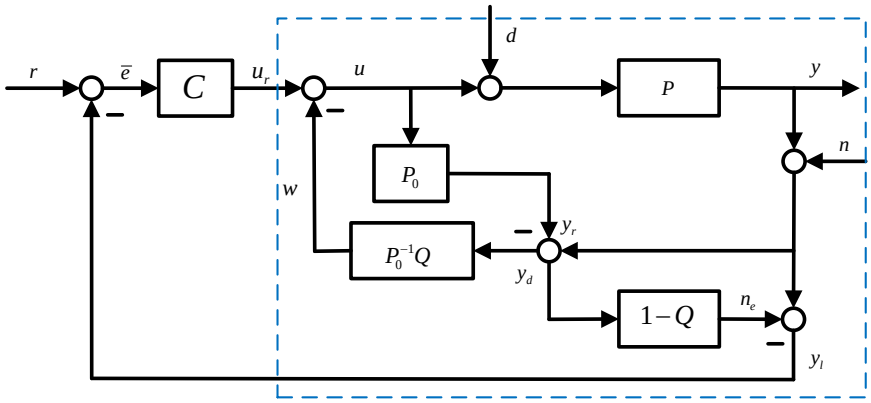

Figure 2. Control system based on NRDOB from [18].

Here P_0 is the nominal model of P, u is the control inputs for the nominal model, and signals r, d, and n represent the reference input, input disturbance, and sensor noise, respectively. According to the above block diagram, it is easy to obtain the following transfer function:

$$\frac{y_l(s)}{u_r(s)} = P(s) \tag{16}$$

Similarly, the transfer function from $u_r(s)$ to $y_l(s)$ is

$$\frac{y_l(s)}{u_r(s)} = \frac{2P}{1+PP_0^{-1}} \tag{17}$$

MNRDOB's feedback node is different from NRDOB, and its function is similar to model reference adaptive control, that is, forcing the behavior of the controlled object to follow the nominal model. Next, the characteristics of MNRDOB will be further elaborated. Calculating the output y and the control input u

$$\begin{aligned} y(s) &= T_{yr}(s)r(s) + T_{yd}(s)d(s) + T_{yn}(s)n(s) \\ u(s) &= T_{ur}(s)r(s) + T_{ud}(s)d(s) + T_{un}(s)n(s) \end{aligned} \tag{18}$$

where

$$T_{ur} = \frac{P_0C(1+Q)}{P_0(1+C(P_0+2PQ\text{-}P_0Q))+PQ}, \quad T_{yr} = PT_u,$$

$$T_{ud} = \frac{-PQ(2P_0C+1)}{P_0(1+C(P_0+2PQ\text{-}P_0Q))+PQ}, \quad T_{yd} = \frac{P_0P\left(1+P_0C-P_0CQ\right)}{P_0(1+C(P_0+2PQ\text{-}P_0Q))+PQ},$$

$$T_{un} = \frac{-Q(1+2P_0C)}{P_0(1+C(P_0+2PQ\text{-}P_0Q))+PQ}, \quad T_{yn} = PT_{un}.$$

Defining the low-pass filter (LPF) $Q(s)$ as

$$Q(s) = \frac{c_h(\tau s)^h + c_{h-1}(\tau s)^{h-1} + \cdots + c_0}{(\tau s)^l + a_{l-1}(\tau s)^{l-1} + \cdots + a_1(\tau s) + a_0} \tag{19}$$

where $h \geq 0$ and $l \geq 0$ are integers, and $\tau > 0$ is a constant. Let $c_0 = a_0$, $r:deg\left(Q((s))\right) \geq r:deg\left(P_n(s)\right)$, and $Q(s)$ is stable.

Suppose that there exists an $\omega_L > 0$ such that the reference input $r(j\omega)$ and disturbance $d(j\omega)$ are large enough in the low frequency range $[0, \omega_L]$, the sensor is noisy $n(j\omega) \approx 0$, and there exists an $\omega_H > \omega_L$ such that $n(j\omega)$ is large enough in the high-

frequency band $[\omega_L, \omega_H]$ and that both $r(j\omega)$ and $d(j\omega)$ are approximately equal to zero. An appropriate LPF $Q(s)$ meets the following simple approximation:

$$\begin{aligned} |Q(j\omega)| &\approx 1, \qquad \omega \in [0, \omega_L] \\ |Q(j\omega)| &\approx 0, \qquad \omega \in [\omega_H, \infty] \end{aligned} \tag{20}$$

If $\omega \in [0, \omega_L]$, from (18) one has

$$T_{yr}(j\omega) \approx \frac{2PP_0C}{P_0 + 2PP_0C + P}(j\omega) = \frac{2PC}{(1 + P/P_0) + 2PC}(j\omega) \tag{21}$$

Supposing that $\lim_{\omega \to 0} P/P_0 = \alpha$ is a positive constant, the MNRDOB control system can accurately track the step reference, which is similar to the nominal control system without the MNRDOB. Similarly, for low frequency disturbances

$$T_{yd}(j\omega) \approx \frac{PP_0}{P_0 + 2PP_0C + P}(j\omega) = \frac{P}{(1 + P/P_0) + 2PC}(j\omega) \tag{22}$$

For the nominal control system, the transfer function between the disturbance and the output is

$$T_{yd}(j\omega) = \frac{P}{1 + PC}(j\omega) \tag{23}$$

Remark 5. *It can be seen from (22) and (23), for nominal controllers without an observer structure, an appropriate P_0 always guarantees that the disturbance rejection of the MNRDOB controller is stronger than the nominal one. As far as ADRC is concerned, the ESO needs to estimate the total disturbance from y_1. However, the filtering effect of $Q(s)$ will filter out some disturbance information, resulting in the ESO's disturbance estimation ability being limited. Therefore, the anti-disturbance capability of the ADRC with NRDOB is weaker than that of ADRC alone. In addition, the ADRC's anti-disturbance capability is negatively correlated with τ of the Q-filter.*

In the high-frequency range $\omega \in [\omega_H, \infty]$,

$$\begin{aligned} T_{yn}(j\omega) &\approx -\frac{PQ(1 + 2P_0C)}{P_0(1 + P_0C)}(j\omega) \approx 0 \\ T_{un}(j\omega) &\approx -\frac{Q(1 + 2P_0C)}{P_0(1 + P_0C)}(j\omega) \approx 0 \end{aligned} \tag{24}$$

Therefore, with an appropriate LPF $Q(s)$, the MNRDOB can effectively attenuate noise.

Remark 6. *As can be seen from Figure 2, the MNRDOB compensates for disturbance by w and suppresses sensor noise by n_e. These two functions of MNRDOB are necessary for controlling a high-order plant with a low-order ADRC. Ideally, $P(s)$ is converted to a reference model $P_0(s)$ by feedback w. For a low-order ADRC, a low-order $P_0(s)$ is expected. Of course, an excessive modeling error may also lead to the loss of system stability.*

3.2. Robust Stability Analysis

The robust stability of the MNRDOB closed-loop system will be discussed in this section. First, considering the following uncertain system set $\wp$,

$$\wp = \left\{ P(s) = \frac{b_0}{a_0 s^n + a_1 s^{n-1} + a_2 s^{n-1} + \ldots + a_n} : a_i \in [\underline{a}_i, \overline{a}_i] \right\} \tag{25}$$

where n is a positive integer, and all $\underline{a}_i$ and $\overline{a}_i$ are known constants. We assume that both the real uncertain plant $P(s)$ and its nominal model $P_0(s)$ belong to $\wp$. Let $P(s) = \frac{N(s)}{D(s)}$, $P_0(s) = \frac{N_0(s)}{D_0(s)}$, and $0 \le \lambda = \deg(D(s)) - \deg(D_0(s)) \le 1$. It is worth noting that (1) and (25) are equivalent, and $b_n = \frac{b_0}{a_0}$.

According to the structure of Figure 3, the nine transfer functions from $[r, d, n]^T$ to $[u, y, \overline{e}]^T$ in are given as follows:

$$\frac{1}{\Delta(s)} \begin{bmatrix} P_0 C(1+Q) & -PQ(2P_0 C+1) & -Q(1+2P_0 C) \\ P_0 PC(1+Q) & P_n P(1+P_0 C - P_0 CQ) & -PQ(1+2P_0 C) \\ P_0 + PQ & -P_0 PQ & -P_0 Q \end{bmatrix} \tag{26}$$

where $\Delta(s) = (1-Q)P_0 C + 1 + Q + 2PCQ$. If the above nine transfer functions are stable, the closed loop system is said to be internally stable. Let $C(s) = \frac{N_C(s)}{D_C(s)}$ and $Q(s) = \frac{N_Q(s)}{D_Q(s)}$, which are ratios of coprime polynomials. Then, (26) can be written as

$$\frac{1}{\delta(s,\tau)} \begin{bmatrix} M_{11} & M_{12} & M_{13} \\ M_{21} & M_{22} & M_{23} \\ M_{31} & M_{32} & M_{33} \end{bmatrix} \tag{27}$$

where $\delta(s;\ \tau) := (DD_0 D_C N_0 + DN_0^2 N_C) D_Q + (2D_0 NN_0 N_C + D_0^2 D_C N - DN_0^2 N_C) N_Q$ and M_{ij} are suitably defined from (19). Therefore, the NRDOB closed-loop system is internally stable if and only if $\delta(s;\ \tau)$ in (27) is Hurwitz for $P(s) \in \wp$, defining $m := deg(DD_0 D_C N_0)$. Then, the equation $\delta(s;\ \tau) = 0$ has $m+l$ roots, because all the transfer functions P, P_0, C, and Q are strictly proper.

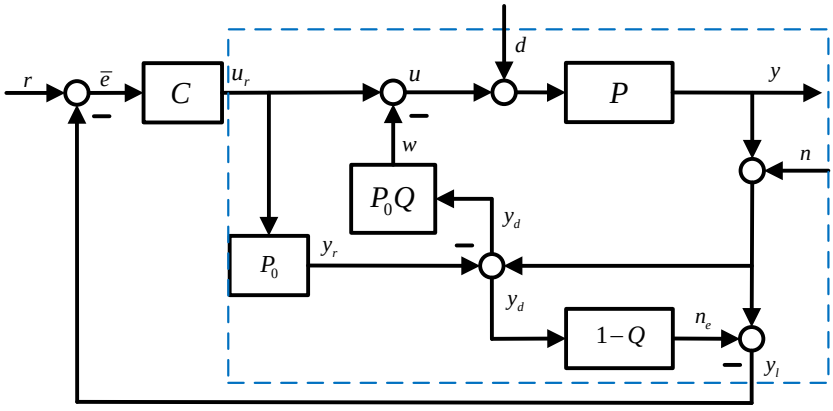

Figure 3. Control system based on MNRDOB.

Lemma 2. *Let*

$$\begin{aligned} P_s(s) &:= D_0(DD_CN_0 + 2NN_0N_C + D_0D_CN) \\ P_f(s) &:= D_Q(s;\,1) + \lim_{s\to\infty}\frac{P(s)}{P_0(s)}N_Q(s;\,1) \end{aligned} \tag{28}$$

There exist m and l roots for $P_s(s)=0$ and $P_f(s)=0$, respectively. Let $s_i^*\ (i=1,\dots,m+l)$ be the roots of $\delta(s;\,\tau)=0$. Then, we have

$$\begin{aligned} &\lim_{s\to\infty} s_i(\tau) = s_i^*, \quad i=1,\dots,m \\ &\lim_{s\to\infty} \tau s_i(\tau) = s_i^*, \quad i=m+1,\dots,m+l \end{aligned} \tag{29}$$

Proof of Lemma 2. Since $D_Q(s;\,0)=N_Q(s;\,0)=a_0\neq 0$, it follows that $\delta(s;\,0)=D_0(DD_CN_0+2NN_0N_C+D_0D_CN)=a_0P_s(s)$. Therefore, m roots of $\delta(s;\,\tau)=0$ converge to those of $P_s(s)=0$ as τ approaches zero. Considering the remaining l roots of $\delta(s;\,\tau)=0$, let

$$\bar{\delta}(s;\,\tau) := \eta_1(s;\,\tau)D_Q(\frac{s}{\tau};\,\tau) + \eta_2(s;\,\tau)N_Q(\frac{s}{\tau};\,\tau) \tag{30}$$

where $\eta_1(s;\,\tau) = \tau^m(DD_0D_CN_0 + DN_0{}^2N_C)\big|_{s=s/\tau}$ and $\eta_2(s;\,\tau) = \tau^m(2D_0NN_0N_C + D_0{}^2D_CN - DN_0{}^2N_C)\big|_{s=s/\tau}$. Because P, P_0, C, and Q are strictly proper and $0\le\lambda=\deg(D(s))-\deg(D_0(s))\le 1$, we have $\lim_{\tau\to 0}\eta_1(s;\,\tau)=\lim_{\tau\to 0}\tau^m DD_0D_CN_0\big|_{s=s/\tau}=\bar{\eta}_1 s^m$ and $\lim_{\tau\to 0}\eta_2(s;\,\tau)=\lim_{\tau\to 0}\tau^{m-\lambda}D_0{}^2D_CN\big|_{s=s/\tau}=\bar{\eta}_2 s^{m-\lambda}$ for all s with some constants $\bar{\eta}_1$ and $\bar{\eta}_2$. Moreover, since $D_Q(s/\tau;\,\tau)=D_Q(s;\,1)$ and $N_Q(s/\tau;\,\tau)=N_Q(s;\,1)$, it follows that $\bar{\delta}(s;\,0)=\bar{\eta}_1 s^m[D_Q(s;\,1)+\frac{\bar{\eta}_2}{s^\lambda\bar{\eta}_1}N_Q(s;\,1)]=\bar{\eta}_1 s^m P_f(s)$. Thus, $\bar{\delta}(s;\,\tau)=0$ have m roots at the origin and l roots at $s_{m+1}^*\cdots s_{m+l}^*$. According to Lemma 1 of [27], there exist l roots for $\bar{\delta}(s;\,\tau)=0$, defining $\bar{s}_i\ (i=1,\dots,m+l)$ such that $\lim_{\tau\to 0}\bar{s}_i(\tau)=s_i^*$. Since $\bar{s}_i(\tau)/\tau$ are the roots of $\delta(s;\,\tau)=0$, (29) is proved. □

Based on Lemma 2, a theory for robust stability of the MNRDOB closed-loop systems is proposed as follows:

Theorem 1. *For all $0<\tau\le\tau^*$ where $\tau^*>0$, the MNRDOB closed-loop system is robustly internally stable if the following three conditions hold:*

(a) $P_0(s)$ is stable; (b) $\dfrac{2PP_0C}{P_0+2PP_0C+P}$ is stable for all $P(s)\in\wp$; (c) $P_f(s)$ is Hurwitz.

Proof of Theorem 1. The denominators of $\dfrac{2PP_0C}{P_0+2PP_0C+P}$ and $P_n(s)$ are $DD_CN_0+2NN_0N_C+D_0D_CN$ and $D_0(s)$, respectively. Thus, (a) and (b) imply that $P_s(s)$ is stable, so the proof follows Lemma 2. □

Remark 7. *For condition (b), the controlled object of the nominal controller $C(s)$ is*

$$P^*(s) = \frac{y_l(s)}{u_r(s)} = \frac{2NN_0}{DN_0 + D_0N} \tag{31}$$

For $n \le 3$, a proper P_0 always guarantees that (31) is stable whether P is stable or not. A stable control object is easy to control. In addition, for $\lambda = 0$, $P_f(s) = D_Q(s;\,1) + \alpha N_Q(s;\,1)$, whose stability needs further verification. In addition, for $\lambda = 1$, since the denominator of $Q(s)$ is the Hurwitz polynomial, $P_f(s) = D_Q(s;\,1)$ is stable. Then, the three stability conditions of the closed-loop system are reduced to two.

The compound control system of ADRC with MNRDOB is shown in Figure 4. It can be seen that the disturbances observed by the MNRDOB are used to improve the structure of the plant $P(s)$ and to cancel the disturbance d. The ADRC's controlled object is $P^*(s)$ modified by the MNRDOB. Therefore, the disturbances suppressed by ADRC are the model errors with $P^*(s)$ and the residual disturbances of d cancelled by the MNRDOB.

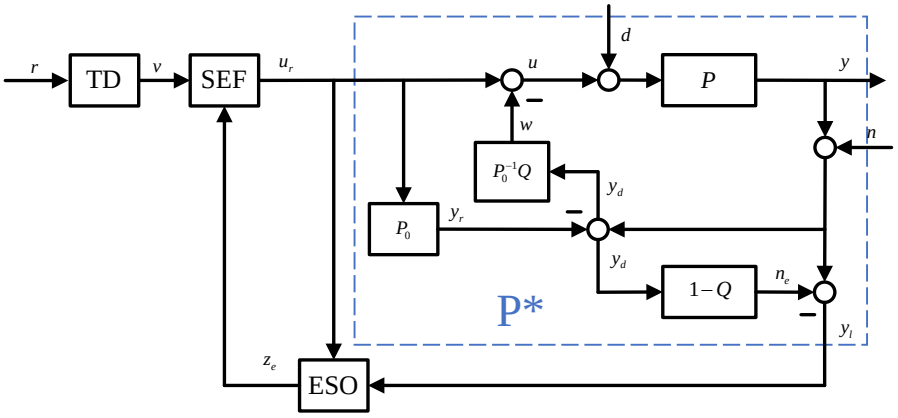

Figure 4. Control system based on ADRC with MNRDOB.

Remark 8. *The NRDOB is first proposed by [18]. However, there are two reasons why the structure of the NRDOB in [18] is not used in this paper. Firstly, the transfer function between disturbance* d *and output* y *is*

$$T_{yd} = \frac{P_0P(1-Q)}{P_0 + Q(P - P_0)} \tag{32}$$

Therefore, its anti-disturbance capability depends only on the NRDOB and has nothing to do with $C(s)$. If ADRC is combined with NRDOB in [18], its advantages in disturbance rejection will be cancelled out. Secondly, for NRDOB in [18], one of the conditions for the robust internal stability is

$$P_f(s) := D_Q(s;\,1) + \left(\lim_{s\to\infty}\frac{P(s)}{P_0(s)} - 1\right)N_Q(s;\,1) \tag{33}$$

For the reduced-order ADRC, $\lambda = 1$ is expected. Obviously, if $\lambda = 1$, in (33), there will be at least one root at the origin. Furthermore, the robustness of the NRDOB system will not be determined.

Note that the design and stability proof of MNRDOB are based on affine system models such as (25), so it cannot be applied to non-affine systems similar to those mentioned in [28].

4. Simulation and Analysis

In this section, some simulation results are used to illustrate the effectiveness of the proposed method. The simulated plant is derived from a speed plant of a one-dimensional gimbal, which is driven directly by a brushless DC motor. Figure 5 shows the equivalent schematic diagram of the one-dimensional gimbal.

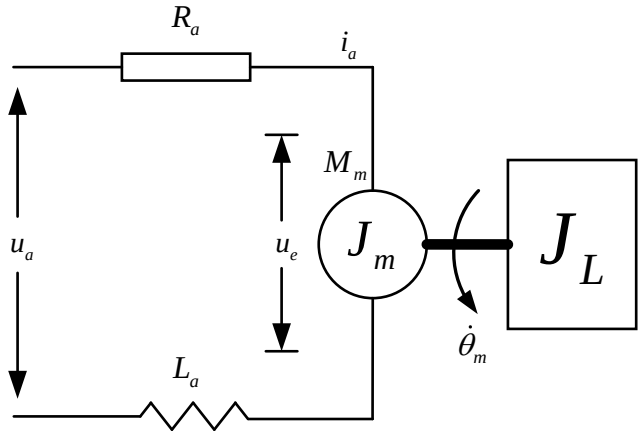

Figure 5. The equivalent schematic diagram of the one-dimensional gimbal.

Here, u_a is the ideal voltage, R_a is the resistance of the armature, L_a is inductance of the armature, i_a is the current of the armature, M_m is the output torque of the motor, u_e is counter electromotive force, $\dot{\theta}_m = \omega_m$ is the angular velocity of the motor, J_m is the inertia of motor, J_L is the inertia of load, and the total inertia of the system is $J = J_m + J_L$. Since the one-dimensional gimbal directly driven by the motor has high transmission stiffness, assuming that only the influence of viscous damping friction is considered, the transfer function from control voltage to angular velocity of the one-dimensional gimbal is

$$\begin{aligned} P(s) &= \frac{\omega_m(s)}{u_a(s)/K_w} \\ &= \frac{K_w C_m}{L_a J s^2 + (L_a B_m + J R_a)s + (R_a B_m + C_e C_m)} \\ &= \frac{b_0}{a_0 s^2 + a_1 s + a_2} \end{aligned} \tag{34}$$

where C_m is the moment coefficient, C_e is the back EMF coefficient, and K_w is the power amplification ratio. The parameters of the one-dimensional gimbal are shown in Table 1.

Table 1. The parameters of the one-dimensional gimbal.

Parameters		
Armature resistance	R_a	2.25 (Ω)
Armature inductance	L_a	0.0067 (H)
Total inertia	J	0.011 (kg × m²)
Back EMF coefficient	C_e	2.67 (V/(rad/s))
Moment coefficient	C_m	4.5 (N m/A)
Viscous damping coefficient	B_m	0.002 (N m/(rad/s))

Power amplification ratio	K_w	5.4

Let us consider some external disturbance $d(t)$, and then the state space form of (34) is

$$\begin{aligned} \dot{x}_1 &= x_2 \\ \dot{x}_2 &= \frac{1}{a_0}\left(-a_2 x_1 - a_1 x_2\right) + b_2 u_r + d \end{aligned} \tag{35}$$

where $x_1 = \omega_m$, $b_2 = \frac{b_0}{a_0}$. Let $f_3 = \frac{1}{a_0}\left(-a_2 x_1 - a_1 x_2\right) + d$ be the total disturbance, and then a second-order ADRC can be designed according to (4) and (5). Based on (11), (35) can be reduced to

$$\dot{x}_1 = \left[x_2 - b_1 u_r\right] + b_1 u_r \tag{36}$$

where $b_1 = \frac{b_0}{a_1}$ and the total disturbance $f_2 = x_2 - b_1 u_r$. Similarly, according to (4) and (5), a first-order ADRC can be obtained. It is worth noting that since (34) is stable, Assumptions 1 and 2 are easily satisfied as long as the reference signal and its derivatives are bounded.

According to the bandwidth tuning method given by [5], the parameters of the two ADRC are set as follows: for the second-order ADRC (SOADRC) $\omega_c = 488$, $\omega_o = 400$, and $b = b_2 = 329660$; and for the first-order ADRC (FOADRC), $\omega_c = 500$, $\omega_o = 400$, and $b = b_1 = 692$. It should be noted that the observation bandwidth of the second-order ESO and the third-order ESO is the same, and the gain of proportional control is also the same, which ensures the fairness of the comparison experiment. In addition, the first-order ADRC still needs TD to arrange the transition process to ensure that the derivative of control input u_r is bounded even if the reference signal is a step signal.

Figure 6 shows the simulation results of the step response, and the 5% sensor noise, which is much more intense than it actually is, is added at $t = 1s$. As shown in Figure 6a, one can see that the response speed of the FOADRC is faster than that of the second-order ADRC, and the time to reach reference of the FOADRC is about 0.07 s, which is about 1/3 of the SOADRC's. To suppress sensor noise, a low-pass filter (LPF) is connected in series on two ADRC controllers, respectively, in Figure 6b, and the LPF is simply chosen as

$$G_{LPF} = \frac{1}{\tau s + 1} = \frac{1}{0.02s + 1} \tag{37}$$

The simulation results show that, when the LPF is added, the FOADRC has significant overshoot (about 45%) and oscillation, while SOADRC maintains good control performance. Although FOADRC is superior in sensor noise suppression, its step response performance and noise suppression capability are significantly reduced after adding LPF. Therefore, FOADRC has lower robustness. These results not only demonstrate the performance of the above methods but also confirm the analysis of the noise and robustness of the reduced-order ADRC in Remark 4.

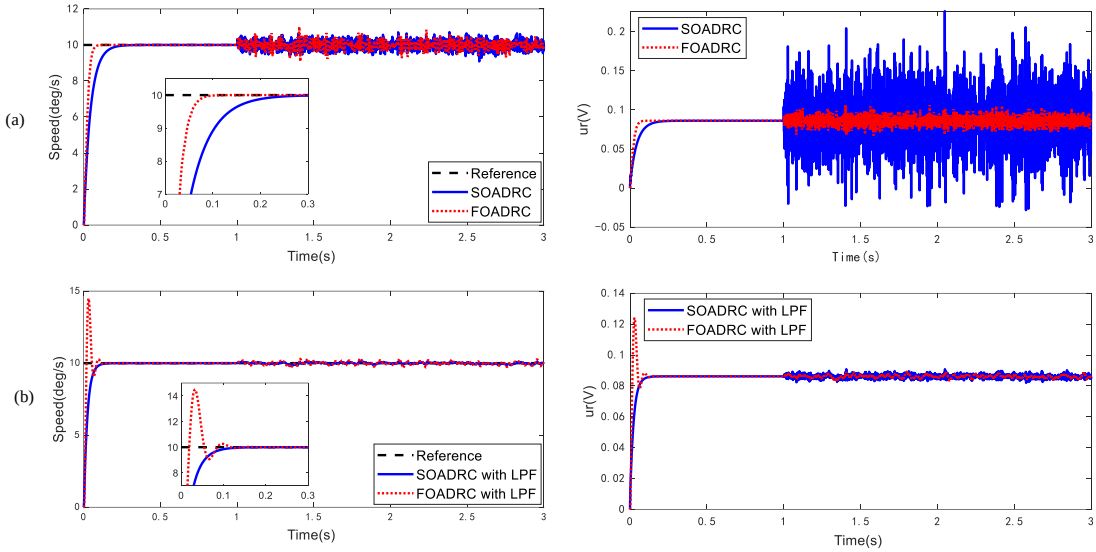

Figure 6. The simulation results of step response. (**a**) Two ADRC; (**b**) Two ADRC with LPF.

In order to verify the superiority of reduced-order ADRC + MNRDOB in robustness and noise suppression, the nominal model $P_0(s)$ is chosen as

$$P_0(s) = \frac{b_0}{a_1 s + a_2} \tag{38}$$

In addition, the Q-filter is simply chosen as (37). The simulation results are shown in Figure 7. One can see that input noise and output noise are effectively suppressed after adding the MNRDOB compared to using the FOADRC only. In addition, the response speed of the system is the same as that without the MNDOB. The influence of noise on the system output and control input of the above five control methods is shown in Table 2 in order to more intuitively show the advantages of reduced-order ADRC + MNRDOB in noise suppression. As can be seen from Table 2, for the FOADRC with MNRDOB, the noise in the control input is the smallest, and the noise in the system output is only slightly greater than the SOADRC with LPF.

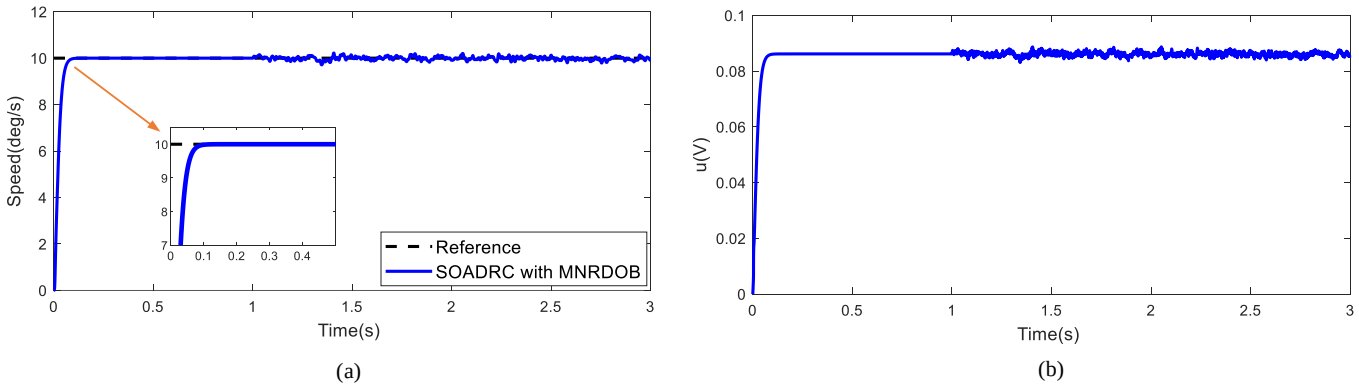

(a) (b)

Figure 7. The simulation result of step response by FOADRC with MNRDOB. (**a**) Speed(deg/s); (**b**) u(V).

Table 2. The impact of sensor noise on different control algorithms.

Control Methods	Noise in System Output (RMS/deg/s)	Noise in Control Input (RMS/V)
SOADRC	0.4079	0.0305
SOADRC with LPF	0.0577	0.0012
FOADRC	0.2298	0.0059
FOADRC with LPF	0.1654	0.0015
FOADRC with MNRDOB	0.0848	0.0008

In order to further verify the enhancement of system robustness by the MNRDOB, the simulation experiment is carried out by increasing and decreasing the inertia and keeping the controller parameters constant. The simulation results of the step response are shown in Figure 8, in which sensor noise is not considered. When a_0 is 1/5 of the original, the step response of the FOADRC and the FOADRC with MNRDOB remains excellent, while the SOADRC oscillates violently. When a_0 increases to five times of the original, the FOADRC loses stability, the SOADRC remains excellent, and the FOADRC with MNRDOB has small oscillation but stabilizes for 0.4 s. Therefore, the composite control strategy of the FOADRC with MNRDOB has more outstanding performance in terms of robustness.

Remark 9. *Note that in practical engineering applications, the higher-order terms with minimal coefficients in the transfer function are usually ignored to simplify the controlled object model. For reduced-order ADRC, the smaller the coefficient of the higher-order term ignored, the better the robustness of the system and vice versa. The simulation experiments in Figure 6 well confirm this statement. The reasons for the improved robustness of FOADRC with MNRDOB can be found in Figure 4 and by (31). The control object of FOADRC is converted from* P *to* P^* *by the MNRDOB; for* P *in (34), based on (31),* P^* *restructured by the MNRDOB by using the nominal model in (38) is*

$$P^*(s) = \frac{2NN_0}{DN_0 + D_0N} = \frac{b_0}{0.5a_0s + a_1s + a_2} \tag{39}$$

Obviously, the coefficient of the second-order term in P^* is reduced by half compared to P, so the compound control strategy of the ADRC with MNRDOB has strong robustness. It should be emphasized that the coefficient of the second-order term in P^* can be reduced by decreasing the numerator of the nominal model P_0, thus further improving the robustness of the system. On the other hand, it can be seen from Equation (24) that reducing the numerator of P_0 can also improve the disturbance suppression ability of the MNRDOB system.

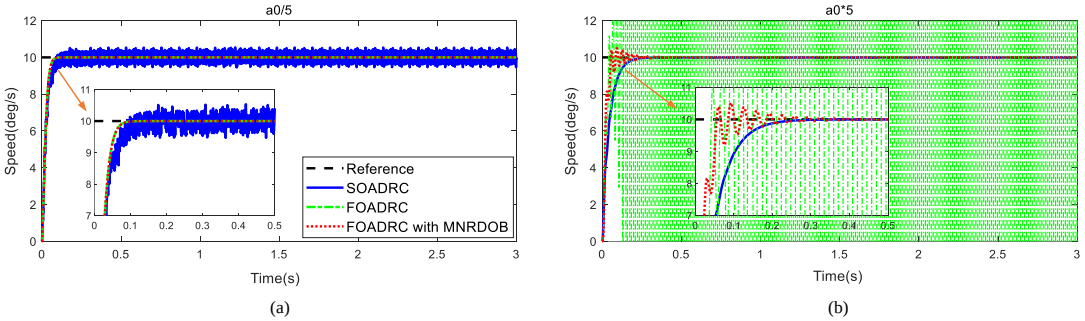

Figure 8. Robustness comparison for three control methods. (**a**) $a_0/5$; (**b**) $5a_0$.

5. Experimental Results

To verify the practicability and validity of the proposed scheme, some experiments are carried out on the experimental setup shown in Figure 9. The control system for the one-dimensional gimbal includes a DSP control board (the control chip is TMS320F283335), PC, and power supply. The sampling frequency of the speed loop is 1 kHz. The main parameters of the plant are consistent with those described in the simulation. The experimental device used in this paper is for aerospace application, which is required to run at a low speed to ensure the stability of spacecraft. Therefore, all the experiments in this paper test the performance of the system at low speed.

In this section, the control performance of the three control methods, second-order ARRC with LPF, FOADRC with NRDOB (from [18]), and FOADRC with MNRDOB, will be compared. The control parameters used in the experiment are consistent with those in the simulation. For NRDOB, since the first-order nominal model cannot guarantee its stability, the nominal model is chosen as model (34), and the corresponding filter Q is selected as a second-order low-pass filter $Q(s) = \frac{1}{(0.02s+1)^2}$. Based on Remark 9, the nominal model for the MNRDOB is designed as (40) to improve the robustness and disturbance rejection ability of the MNRDOB system to improve the robustness and disturbance rejection ability of the MNRDOB system

$$P_0(s) = \frac{b_0/3}{a_1 s + a_2} \tag{40}$$

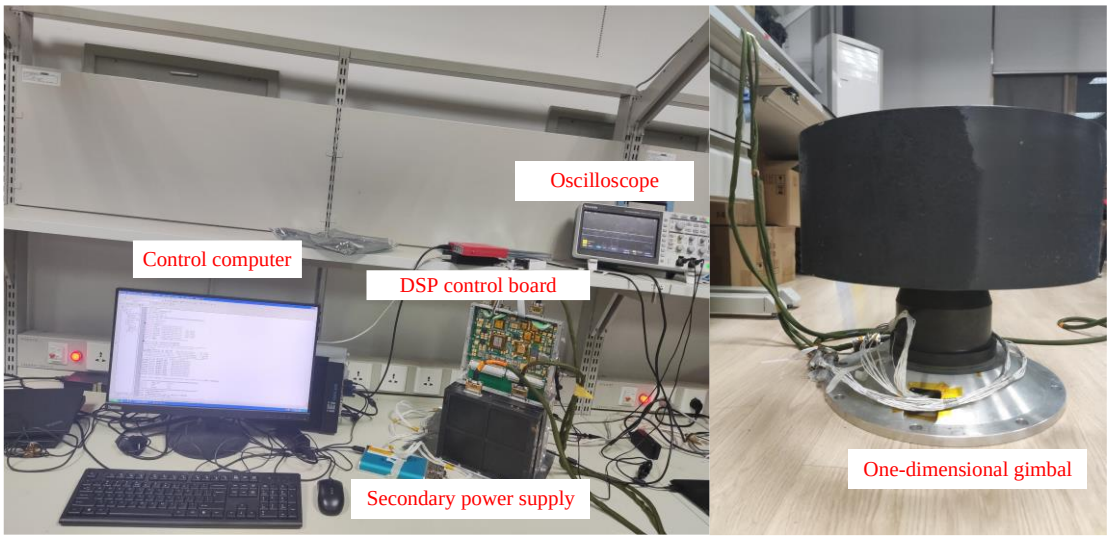

Figure 9. Experimental setup.

Figure 10 shows the step responses and sinusoidal disturbance suppression effects of the three controllers, in which the sinusoidal control voltage disturbances of $0.1\sin(2\pi t)$ and $0.05\sin(10\pi t)$ are added at $t = 1s$, respectively. One can see that the FOADRC with MNRDOB has the strongest ability to suppress sinusoidal disturbances, the FOADRC with NRDOB has the second, and the SOARRC with LPF has the weakest. In order to further verify the disturbance inhibition of the proposed method, in the experiment shown in Figure 11, a step control input disturbance $d = 1V$ and a step disturbance $d = 0.1\text{rad/s}$ were added at 1 s and 2.5 s, respectively. The results show that the proposed method can force the system to reconverge faster to the reference trajectory under the same disturbance conditions. In addition, the response speed of the SOADRC with LPF is slower than the other two methods. Therefore, the proposed methods are outstanding in the step response and disturbance inhibition.

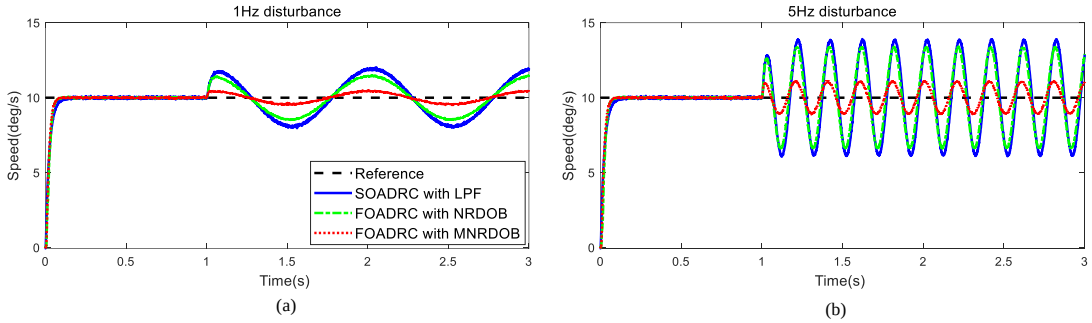

Figure 10. Experimental results of the step response and sinusoidal disturbance. (**a**) 1 Hz disturbance; (**b**) 5 Hz disturbance.

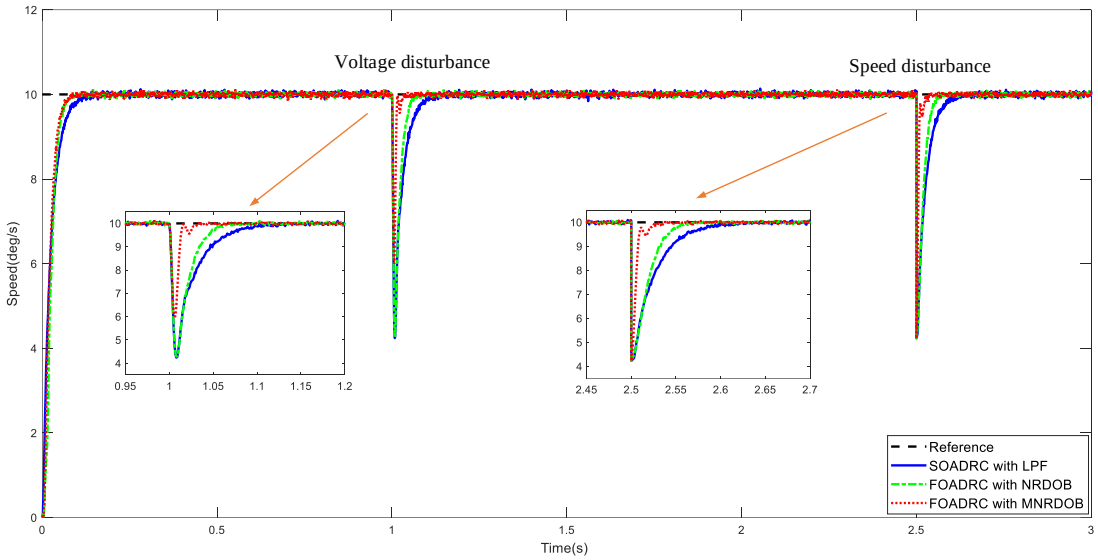

Figure 11. Experimental results of step disturbance.

Figure 12 shows the tracking results of the three control methods at different speeds (5 deg/s, 15 deg/s, and 25 deg/s). It can be seen that the step response performance of the three control methods at different speeds is consistent with the results in Figure 11. Therefore, the proposed method has good control performance at different speeds.

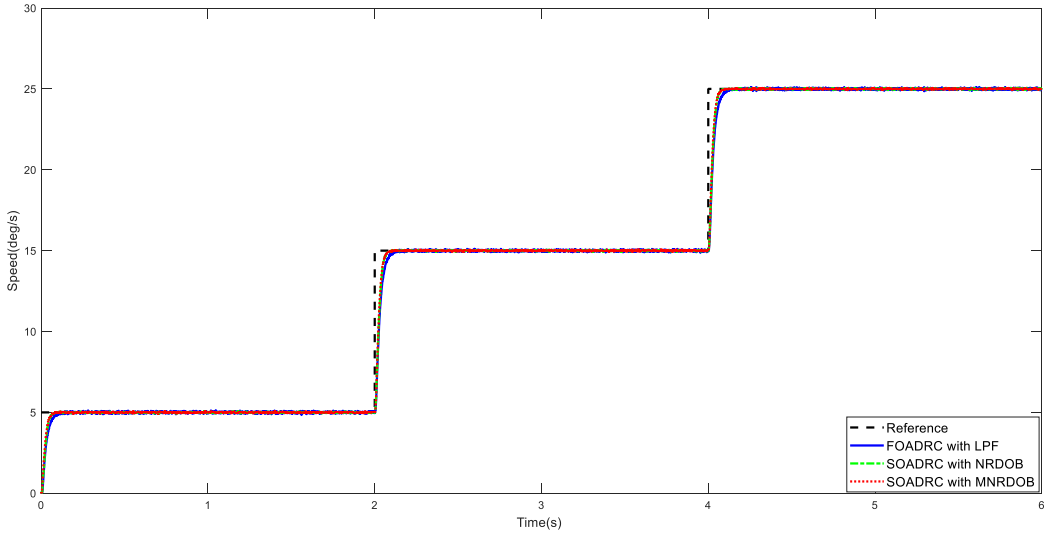

Figure 12. Experimental results of different speed references.

To verify the advantages of the proposed method in tracking performance and friction suppression, a delay compensation of 0.027 s is added to eliminate the influence of phase delay. The experimental results for the sine signal $\sin(\pi t)$ and mixed signal (composed by $2\sin(\pi t)$, $0.5\sin(4\pi t)$, and $0.05\sin(10\pi t)$) are shown in Figures 13 and 14, where the tracking responses and tracking errors are all illustrated, to display the tracking performance of the proposed method. As shown in Figures 13 and 14, the proposed method FOADRC with MNRDOB can retain significantly superior tracking performance than the other two methods in both cases, because the disturbance and the unknown dynamics are better estimated and compensated by the proposed method. As can be seen from the tracking errors in Figures 13 and 14, the proposed method can effectively inhibit the peak error produced by friction compared with the other two methods. The more detailed comparison results are shown in Table 3.

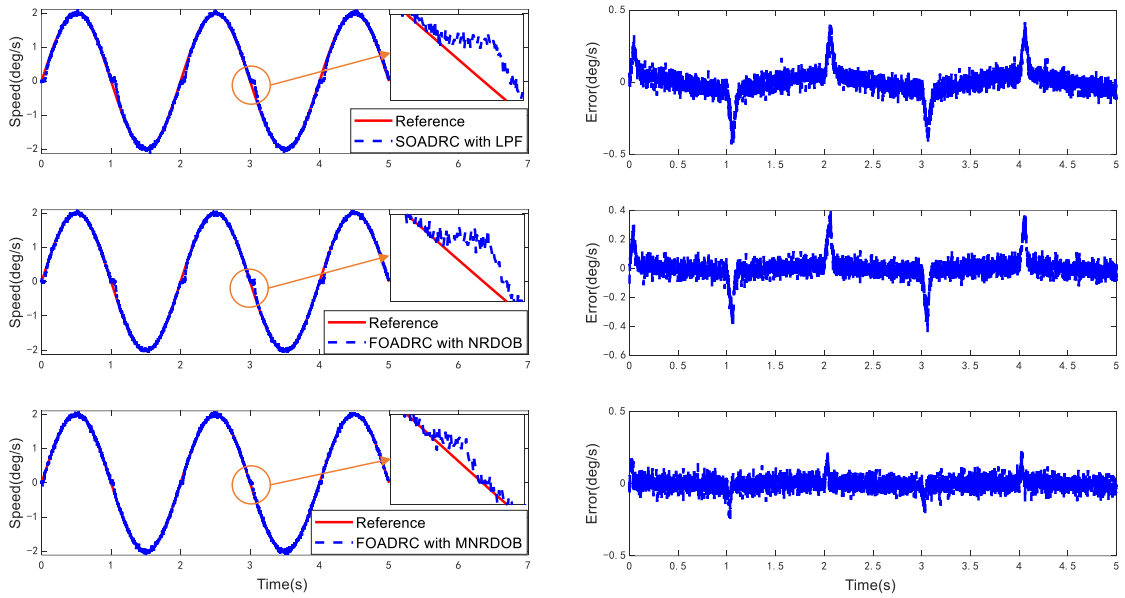

Figure 13. Experimental results of the sinusoidal response. (**a**) Speed(deg/s); (**b**) Error(deg/s).

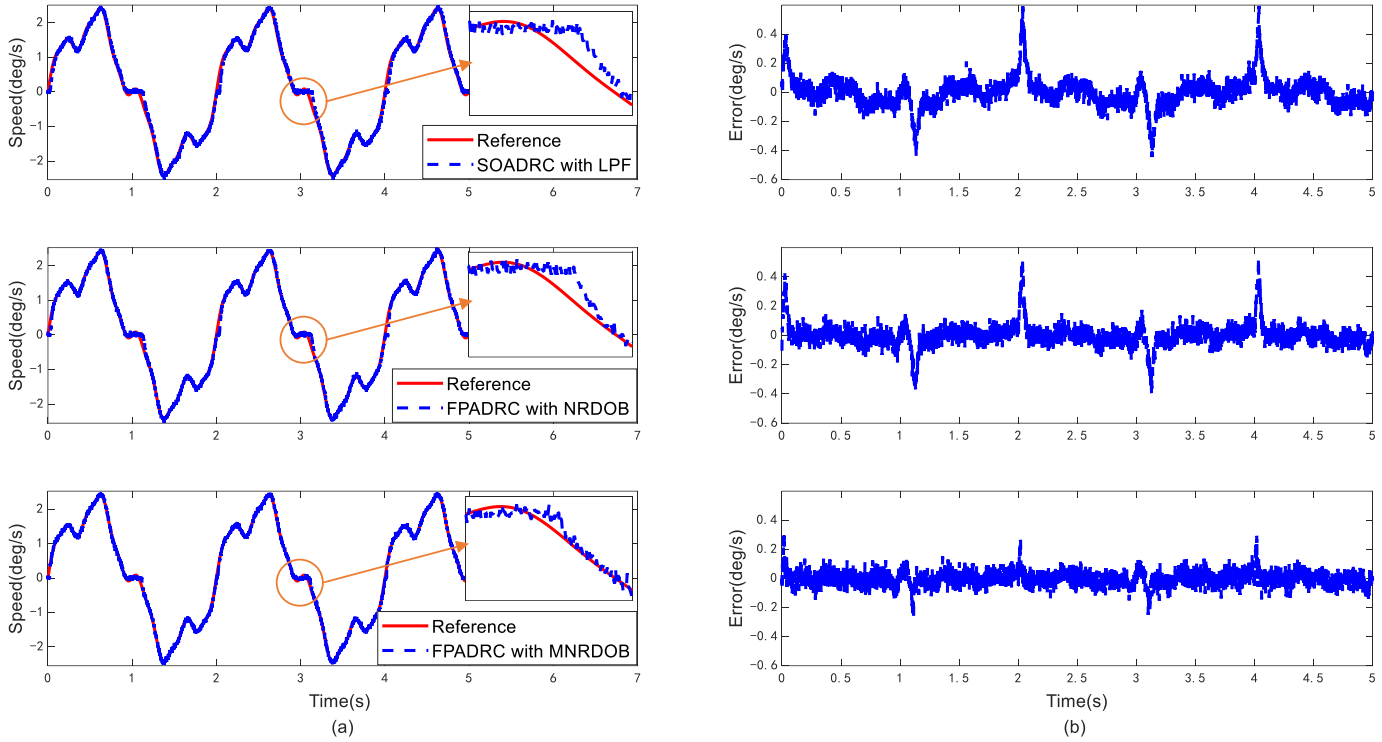

Figure 14. Experimental results of the mixed signal response. (**a**) Speed(deg/s); (**b**) Error(deg/s).

Table 3. Performance comparison of three control methods.

Control Methods	Maximum Tracking Error (deg/s)		Tracking Error (deg/s)			
	Sinusoidal Disturbance		Sine Signal		Mixed Signal	
	1 Hz	5 Hz	Maximum	RMS	Maximum	RMS
SOADRC with LPF	2.021	3.914	0.416	0.0897	0.594	0.1043
FOADRC with NRDOB	1.537	3.462	0.397	0.0739	0.539	0.0865
FOADRC with MNRDOB	0.531	1.169	0.254	0.0485	0.292	0.0560

In recent years, many scholars have proposed many effective control methods for motor speed control, such as model reference adaptive control [29], model predictive control [30], singular perturbation control [31], and neural network method [32], etc. However, the design and algorithm complexity of these methods are high and difficult to implement in engineering. The sliding mode observer (SMO) mentioned in [33] has attracted wide attention due to its high robustness. To further demonstrate the control performance of the proposed method, the results for mixed signal response by sliding mode ESO (SMESO) are shown in Figure 15. The SMESO is the second-order ESO modified to the following form according to SMO in literature [33]:

$$\begin{aligned} \dot{z}_1 &= z_2 - \beta_1 sign(e_1) \\ \dot{z}_2 &= z_3 + b_2 u_r - \beta_2 sign(e_1) \\ \dot{z}_3 &= -\beta_3 sign(e_1) \end{aligned} \tag{41}$$

where $\beta_i, i = 1,2,3$ are the observer gains. For simplicity, the feedback control law and the controller parameters are consistent with the SOADRC.

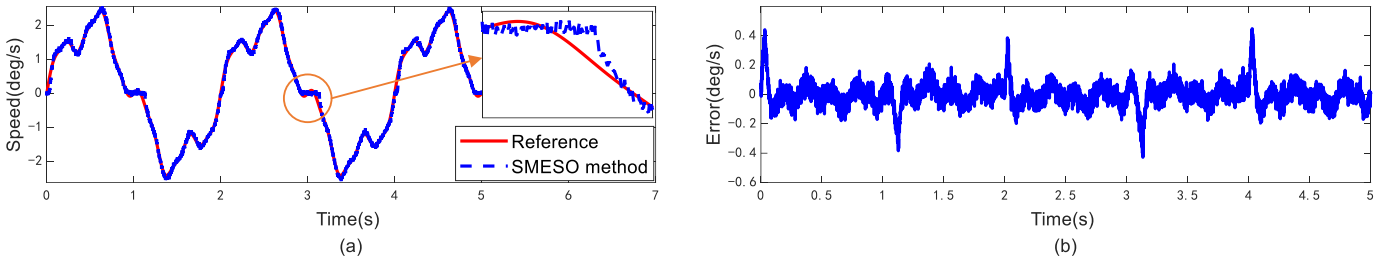

Figure 15. Experimental results of the mixed signal response by SMESO method. (**a**) Speed(deg/s); (**b**) Error(deg/s).

Comparing Figure 14 with Figure 15, we can see that SMESO's tracking performance is better than that of SOADRC with LPF and FOADRC with NRDOB but still not as good as the proposed method. The maximum tracking error of the SMESO method for mixed signals is 0.449 deg/s, and the tracking error RMS is 0.0838 deg/s. In addition, the tracking error of the SMESO method has more fluctuation, which may be caused by chattering of the sliding mode.

6. Conclusions

This paper presents a robust reduced-order method for active disturbance rejection control (ADRC) to achieve high control performance. Frequency domain analysis shows that the lower-order extended state observer (ESO) has stronger disturbance estimation ability. However, direct reduced-order control will reduce the robustness of the system. In addition, the influence of sensor noise is unavoidable in many control systems. Therefore, a modified noise reduction disturbance observer (MNRDOB) is proposed to improve the robustness of the reduced-order ADRC and suppress the sensor noise. Simulation results are presented to illustrate the superiority of the proposed method in robustness and noise reduction. Finally, the effectiveness of the proposed method is verified by speed control of a one-dimensional gimbal, and the results show that the proposed method is excellent in overshoot, rapidity, and disturbance attenuation. Further robustness and stability of the reduced-order ADRC method will be studied in future work.

Author Contributions: Conceptualization, F.W. and P.L.; data curation, Y.C.; formal analysis, P.L.; funding acquisition, M.X.; investigation, F.W.; methodology, F.W.; project administration, B.L.; resources, C.M.; software, P.L.; supervision, M.X.; validation, F.W. and P.L.; visualization, F.J.; writing—original draft, F.W.; writing—review and editing, P.L., F.W., and P.L. contributed equally to this work. All authors have read and agreed to the published version of the manuscript.

Funding: This research received no external funding.

Acknowledgments: Thanks to Tianji Cheng for his help in method design and suggestions on paper writing.

Conflicts of Interest: The authors declare no conflict of interest.

References

1. Gao, Z. Active disturbance rejection control for nonlinear fractional-order systems. *Int. J. Robust Nonlinear Control* **2015**, *26*, 876–892. https://doi.org/10.1002/rnc.3344.
2. Behzad, A.; Amin, N. Hardware Implementation of an ADRC Controller on a Gimbal Mechanism. *IEEE Trans. Control Syst. Technol.* **2018**, *26*, 2268–2275.
3. Han, J. Active disturbance rejection controller and its applications. *Control. Decis.* **1998**, *13*, 19–23. (In Chinese)
4. Han, J. From PID to Active Disturbance Rejection Control. *IEEE Trans. Ind. Electron.* **2009**, *56*, 900–906. https://doi.org/10.1109/tie.2008.2011621.
5. Gao, Z. Scaling and Bandwidth-Parameterization Based Controller Tuning. In Proceedings of the 2003 American Control Conference, Denver, CO, USA, 4–6 June 2003; pp. 4989–4996. https://doi.org/10.1109/acc.2003.1242516.
6. Yin, Z.; Du, C.; Liu, J.; Sun, X.; Zhong, Y. Research on Auto disturbance Rejection Control of Induction Motors Based on an Ant Colony Optimization Algorithm. *IEEE Trans. Electron.* **2018**, *65*, 3077–3094.

7. Qu, L.; Qiao, W.; Qu, L. Active-Disturbance-Rejection-Based Sliding-Mode Current Control for Permanent-Magnet Synchronous Motors. *IEEE Trans. Power Electron.* **2021**, *36*, 751–760.
8. Garrido, R.; Luna, L. Robust ultra-precision motion control of linear ultrasonic motors: A combined ADRC-Luenberger observer approach. *Control Eng. Pract.* **2021**, *111*, 104812.
9. Huang, Z.; Liu, Y.; Zheng, H.; Wang, S.; Ma, J.; Liu, Y. A self-searching optimal ADRC for the pitch angle control of an underwater thermal glider in the vertical plane motion. *Ocean Eng.* **2018**, *159*, 98–111. https://doi.org/10.1016/j.oceaneng.2018.04.010.
10. Guo, T.; Song, D.; Li, K.; Li, C.; Yang, H. Pitch Angle Control with Model Compensation Based on Active Disturbance Rejection Controller for Underwater Gliders. *J. Coast. Res.* **2020**, *36*, 424. https://doi.org/10.2112/jcoastres-d-19-00050.1.
11. Meng, Q.; Hou, Z. Active Disturbance Rejection Based Repetitive Learning Control with Applications in Power Inverters. *IEEE Trans. Control. Syst. Technol.* **2021**, *29*, 2038–2048.
12. Huang, D.; Min, Y.; Jian, Y.; Li, Y. Current-Cycle Iterative Learning Control for High-Precision Position Tracking of Piezo-electric Actuator System via Active Disturbance Rejection Control for Hysteresis Compensation. *IEEE Trans. Ind. Electron.* **2020**, *67*, 8680–8690.
13. Yue, M.; An, C.; Li, Z. Constrained Adaptive Robust Trajectory Tracking for WIP Vehicles Using Model Predictive Control and Extended State Observer. *IEEE Trans. Syst. Man, Cybern. Syst.* **2016**, *48*, 733–742. https://doi.org/10.1109/tsmc.2016.2621181.
14. Shyu, K.-K.; Lai, C.-K.; Tsai, Y.-W.; Yang, D.-I. A newly robust controller design for the position control of permanent-magnet synchronous motor. *IEEE Trans. Ind. Electron.* **2002**, *49*, 558–565. https://doi.org/10.1109/tie.2002.1005380.
15. Qi, L.; Shi, H. Adaptive position tracking control of permanent magnet synchronous motor based on RBF fast terminal sliding mode control. *Neurocomputing* **2013**, *115*, 23–30. https://doi.org/10.1016/j.neucom.2012.11.018.
16. Sira-Ramírez, H.; Zurita-Bustamante, E. On the equivalence between ADRC and Flat Filter based controllers: A frequency domain approach. *Control Eng. Pract.* **2020**, *107*, 104656. https://doi.org/10.1016/j.conengprac.2020.104656.
17. Ren, C.; Li, X.; Yang, X.; Ma, S. Extended State Observer-Based Sliding Mode Control of an Omnidirectional Mobile Robot With Friction Compensation. *IEEE Trans. Ind. Electron.* **2019**, *66*, 9480–9489. https://doi.org/10.1109/tie.2019.2892678.
18. Jo, N.H.; Jeon, C.; Shim, H. Noise Reduction Disturbance Observer for Disturbance Attenuation and Noise Suppression. *IEEE Trans. Ind. Electron.* **2016**, *64*, 1381–1391. https://doi.org/10.1109/tie.2016.2618858.
19. Wang, F.; Wang, R.; Liu, E.; Zhang, W. Stabilization Control Mothed for Two-Axis Inertially Stabilized Platform Based on Active Disturbance Rejection Control with Noise Reduction Disturbance Observer. *IEEE Access* **2019**, *7*, 99521–99529. https://doi.org/10.1109/access.2019.2930353.
20. Zheng, Q.; Gaol, L.Q.; Gao, Z. On Stability Analysis of Active Disturbance Rejection Control for Nonlinear Time-Varying Plants with Unknown Dynamics. In Proceedings of the 2007 46th IEEE Conference on Decision and Control, New Orleans, LA, USA, 12–14 December 2007; pp. 3501–3506. https://doi.org/10.1109/cdc.2007.4434676.
21. Ye, J.; Roy, S.; Godjevac, M.; Baldi, S. A Switching Control Perspective on the Offshore Construction Scenario of Heavy-Lift Vessels. *IEEE Trans. Control Syst. Technol.* **2021**, *29*, 470–477.
22. Roy, S.; Baldi, S.; Ioannou, P.A. An Adaptive Control Framework for Underactuated Switched Euler-Lagrange Systems. *IEEE Trans. Autom. Control* **2021**, *PP*, 1–1. https://doi.org/10.1109/tac.2021.3108507.
23. Godbole, A.; Kolhe, J.; Talole, S. Performance Analysis of Generalized Extended State Observer in Tackling Sinusoidal Disturbances. *IEEE Trans. Control Syst. Technol.* **2013**, *21*, 2212–2223.
24. Moura, J.T.; Elmali, H.; Olgac, N. Sliding Mode Control with Sliding Perturbation Observer. *J. Dyn. Syst. Meas. Control* **1997**, *119*, 657–665. https://doi.org/10.1115/1.2802375.
25. Ohnishi, K.; Shibata, M.; Murakami, T. Motion control for advanced mechatronics. *IEEE/ASME Trans. Mechatron.* **1996**, *1*, 56–67. https://doi.org/10.1109/3516.491410.
26. Asignacion, A.; Haninger, K.; Oh, S.; Lee, H. High-Stiffness Control of Series Elastic Actuators Using a Noise Reduction Disturbance Observer. *IEEE Trans. Ind. Electron.* **2021**, *69*, 8212–8219. https://doi.org/10.1109/tie.2021.3106016.
27. Shim, H.; Jo, N.H. An almost necessary and sufficient condition for robust stability of closed-loop systems with disturbance observer. *Automatica* **2009**, *45*, 296–299. https://doi.org/10.1016/j.automatica.2008.10.009.
28. Zhu, Q. Complete model-free siding mode control (CMFSMC). *Sci. Rep.* **2021**, *111*, 22565.
29. Nguyen, A.T.; Rafaq, M.S.; Choi, H.H.; Jung, J.-W. A Model Reference Adaptive Control Based Speed Controller for a Surface-Mounted Permanent Magnet Synchronous Motor Drive. *IEEE Trans. Ind. Electron.* **2018**, *65*, 9399–9409. https://doi.org/10.1109/tie.2018.2826480.
30. Zhang, Y.; Yin, Z.; Li, W.; Liu, J. Adaptive Sliding-Mode-Based Speed Control in Finite Control Set Model Predictive Torque Control for Induction Motors. *IEEE Trans. Power Electron.* **2020**, *36*, 8076–8087. https://doi.org/10.1109/tpel.2020.3042181.
31. Alfehaid, A.A.; Strangas, E.G.; Khalil, H.K. Speed Control of Permanent Magnet Synchronous Motor With Uncertain Parameters and Unknown Disturbance. *IEEE Trans. Control Syst. Technol.* **2020**, *29*, 2639–2646. https://doi.org/10.1109/tcst.2020.3026569.
32. Yang, Z.; Wang, D.; Sun, X.; Wu, J. Speed sensorless control of a bearingless induction motor with combined neural network and fractional sliding mode. *Mechatronics* **2021**, *82*, 102721. https://doi.org/10.1016/j.mechatronics.2021.102721.
33. Sami, I.; Ullah, S.; Basit, A.; Ullah, N.; Ro, J.-S. Integral Super Twisting Sliding Mode Based Sensorless Predictive Torque Control of Induction Motor. *IEEE Access* **2020**, *8*, 186740–186755. https://doi.org/10.1109/access.2020.3028845.